Macromolecules
ARTICLE

Macromolecules **2009**, *42*, 5709–5716 **5709**
DOI: 10.1021/ma900831h

Effect of Pressure on the Phase Behavior and Segmental Dynamics in Blends of Polystyrene with Poly(methylphenyl siloxane)

Antonis Gitsas and George Floudas*

University of Ioannina, Department of Physics, P.O. Box 1186, 451 10 Ioannina, Greece and Foundation for Research and Technology-Hellas (FORTH), Biomedical Research Institute (BRI)

Ronald P. White and Jane E. G. Lipson*

Department of Chemistry, 6128 Burke Laboratory, Dartmouth College, Hanover, New Hampshire 03755

Received April 16, 2009; Revised Manuscript Received June 18, 2009

ABSTRACT: The effect of pressure on the segmental dynamics in two symmetric blends of PMPS and PS is studied for pressures up to 250 MPa. In these blends, there is interplay between spinodal decomposition and glass transition, resulting in the enrichment of the high T_g component by the more mobile component. The distinctly different pressure sensitivities of PS and PMPS are used as fingerprints of the phase state, allowing for identification of the origin of the two dynamic processes arising from the PMPS segmental dynamics in PMPS-rich and PS-rich domains. Model calculations using a lattice-based equation of state lead to prediction of the phase diagram, as well as the effect of pressure on the critical temperature for the same PS/PMPS blend. The weak pressure sensitivity of the critical temperature (dT_c/dP), compared to the two segmental relaxations, suggests that a transition to a thermodynamically miscible but dynamically heterogeneous state takes place for pressures above 300 MPa.

1. Introduction

The dynamics of polymer blends has attracted the interest of the scientific community for a number of years as a result of some unanticipated experimental findings. For example, thermodynamically miscible polymer blends exhibit heterogeneous dynamics, i.e., distinctly different component dynamics at the segmental level.[1−7] A key parameter that can enhance the dynamic heterogeneity is the disparity in the glass temperature (T_g) of the homopolymers i.e., the difference between the component glass temperatures, ΔT_g, known as dynamic asymmetry.[8] Systems with even a modest dynamic asymmetry can result in the breakdown of the empirical time−temperature superposition when probed by rheological[8] or dielectric[5] means. Different models proposed to account for this effect emphasize either intermolecular concentration effects through the concentration fluctuation approach,[9] intramolecular effects through the chain connectivity,[10] or combinations of both.[11−16]

These observations have motivated numerous studies of the thermodynamics and dynamics of polymer blends. Although the effect of pressure, with its relevance in polymer blend processing, is much less investigated, there are some recent experimental[17−26] and theoretical[27,28] efforts that focus on the effects of pressure on the dynamic heterogeneity and phase behavior. With respect to the issue of dynamic heterogeneity, there have been two studies in athermal polymer blends/copolymers: polyisoprene-*b*-poly(vinyl ethylene) (PI-*b*-PVE) ($\Delta T_g \approx 60$ K)[17] and poly(methyl methacrylate)/poly(ethylene oxide) (PMMA/PEO) ($\Delta T_g \approx 180$ K).[18] In the former, an increase in pressure induces dynamic homogeneity, i.e., brings the two segmental time-scales closer, whereas in the latter, the dynamics of the high T_g component (PMMA) under pressure were compatible with the predictions of the self-concentration model. Subsequently, the effect of pressure was investigated with dielectric spectroscopy (DS) in two miscible (but not athermal) blends: polystyrene/poly(vinyl methyl ether) (PS/PVME) ($\Delta T_g \approx 125$ K)[19−22] and in poly(cyclohexyl methacrylate)/poly(α-methyl styrene) (PCHMA/PαMS) ($\Delta T_g \approx 8$ K),[23] having practically one polar component (PVME, PCHMA). Other miscible blends include components with large dynamic asymmetry ($\Delta T_g > 150$ K) where miscibility is induced by hydrogen bonds. Two such blends of poly(vinyl ethyl ether) with poly(4-vinyl phenol)[24] and poly(ethylene-*co*-vinyl acetate)[25] were investigated as a function of pressure. In the former, pressure restores in part the dynamic heterogeneity due to the weakening of hydrogen bonds. On the other hand, in the nanophase-separated diblock copolymer poly(vinyl methyl ether)-*b*-poly(isobutyl vinyl ether) with a minimal dynamic asymmetry ($\Delta T_g \approx 7$ K)[26] the effect of pressure was to enhance the dynamic asymmetry reflecting differences in the local packing of the respective homopolymers.

Polymer blends that phase separate upon lowering (increasing) the temperature thus exhibit an upper (lower) critical solution temperature or UCST (LCST). The effect of pressure on blend miscibility is more interesting in the case of a UCST blend. In this case, the enthalpy change on mixing is positive and pressure can increase or decrease the miscibility depending on the sign of the volume change on mixing.[27,28] An example of a UCST blend with large dynamic asymmetry ($\Delta T_g \approx 113$ K at $P = 0.1$ MPa) is the polystyrene/poly(methyl phenyl siloxane) (PS/PMPS) system. The miscibility and segmental dynamics have been investigated at atmospheric pressure[29,30] and depending on the molecular weight they were found to exhibit dynamic heterogeneity. In addition, the glass temperature, T_g, of the hard phase (PS), interferes with the demixing process, thus giving rise to pinning of the domain structure at a certain stage. Specific information on

*Corresponding author. E-mail: gfloudas@cc.uoi.gr (G.F.); Jane.E.G.Lipson@Dartmouth.edu (J.E.G.L.).

Published on Web 07/02/2009

Table 1. Molecular Characteristics of the Homopolymers

$M_{w,PS}$ (g/mol)	N_{PS}	M_w/M_n (PS)	$M_{w,PMPS}$ (g/mol)	N_{PMPS}	M_w/M_n (PMPS)
5030	48	1.07	2347	17	1.20
2940	28	1.05			

Table 2. Molecular Characteristics of the Blends

blend	N_{PS}	N_{PMPS}	w_{PS}	φ_c[a]
$PS_{48}/PMPS_{17}$	48	17	0.50	0.63
$PS_{28}/PMPS_{17}$	28	17	0.50	0.56

[a] $\varphi_c = (N_{PS})^{1/2}/((N_{PS})^{1/2} + (N_{PMPS})^{1/2})$.

the evolution of phase separation and the degree of purity of phases can be provided by probing the dynamics at the segmental level by DS.

Herein, we focus on two PS/PMPS blends and study the segmental dynamics with dielectric spectroscopy as a function of pressure for pressures up to 250 MPa. The pressure coefficient of the two dynamic processes can be employed as a fingerprint of the purity of phases. In parallel we make use of a lattice-based theoretical model to predict the phase diagram and the effect of pressure on the critical temperature. The aim is to understand the effect of pressure on the complex segmental dynamics in relation to the phase state. To this end, we are interested in comparing the pressure coefficient of the critical temperature with the corresponding coefficients of the dynamic processes. On the basis of this comparison, conclusions can be made on the miscibility and dynamic heterogeneity of the blends as a function of pressure.

2. Experimental Section

Materials and Characterization. The PMPS and PS homopolymers used in the present study were purchased from Polymer Source Inc. and the molecular characteristics are given in Table 1. Molecular weights were determined by size exclusion chromatography. Two symmetric blends of PS/PMPS were made by dissolving both polymers in a 95% w/w toluene. Solutions were stirred for more than 6 h and the solvent was slowly removed by evaporation at ambient temperature. Uniform bubble-free films were prepared by drying in a desiccator at 373 K for 1 week. Traces of solvent were further removed by drying under vacuum at 373 K. The PS mass fraction in the blends is given in Table 2.

Differential Scanning Calorimetry (DSC). A Mettler Toledo Star DSC capable of programmed cyclic temperature runs over the range 113−673 K was used. The samples were first heated at a rate of 10 K/min from ambient temperature to 473 K and then cooled to 173 K with the same rate. A second heating/cooling run with the same rate revealed a broad glass region with an estimated glass temperature, $T_g \approx 261$ K, and ΔT_g of 47 K for the $PS_{28}/PMPS_{17}$ blend and a $T_g \approx 263$ K and ΔT_g of 60 K for the $PS_{48}/PMPS_{17}$ blend.

Dielectric Spectroscopy (DS). Dielectric measurements were made under "isobaric" conditions as a function of temperature and under "isothermal" conditions as a function of pressure. All measurements were performed using a Novocontrol BDS system composed of a Solartron Schlumberger FRA 1260 frequency response analyzer and a broadband dielectric converter for the range 1×10^{-2} to 1×10^{6} Hz. The temperature for the atmospheric pressure measurements was stabilized by a Novocontrol Quatro cryosystem with N_2 flow and a precision of 0.05 K. The "isobaric" measurements were performed at different temperatures in the range 123−370 K, at atmospheric pressure. Measurements were made by cooling from 373 K. A waiting time of 2 h was set prior to each measurement temperature to ensure proximity to "equilibrium". A repeated cycle with the same conditions gave identical results. The "isothermal" measurements were made for temperatures in the range from 298 to 363 K and for pressure up to 300 MPa. The measurements under hydrostatic pressure were carried out in a Novocontrol pressure cell. The pressure setup consists of a temperature controlled cell, hydraulic closing press with air pump, and air pump for hydrostatic test pressure. The sample cell is isolated with a Teflon ring from the surrounding silicon oil that is the pressure transmitting liquid. The "isothermal" frequency sweeps were made with a temperature stability better than ±0.1 K, and a pressure stability better than ±2 MPa.

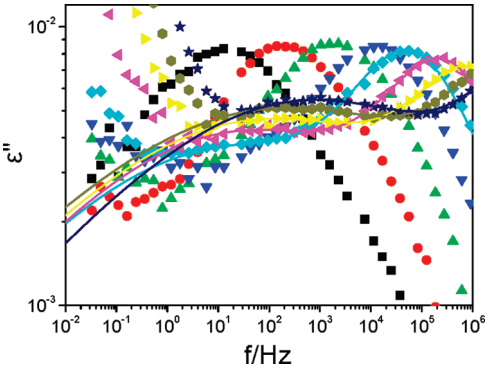

Figure 1. Dielectric loss curves for the $PS_{48}/PMPS_{17}$ blend at 0.1 MPa shown at different temperatures: (squares) 230.15; (circles) 235.15; (up triangles) 240.15; (down triangles) 245.15 K; (rhombus) 250.15; (left triangles) 255.15; (right triangles) 260.15; (polygons) 265.15; and (stars) 270.15 K. The lines are fits to two HN functions.

In every case, the complex dielectric permittivity $\varepsilon^* = \varepsilon' - i\varepsilon''$, where ε' is the real and ε'' the imaginary part, was obtained as a function of frequency ω, temperature T, and pressure P, i.e., $\varepsilon^*(T, P,\omega)$. The analysis of both T- and P-dependent experiments was made using the empirical equation of Havriliak and Negami (HN)[31]

$$\varepsilon^*(T,P,\omega) = \varepsilon_\infty(T,P) + \frac{\Delta\varepsilon(T,P)}{[1+(i\omega\tau_{HN}(T,P))^m]^n} + \frac{\sigma_0(T,P)}{i\varepsilon_f\omega} \quad (1)$$

where ε_∞ (T,P) is the high-frequency permittivity, $\tau_{HN}(T,P)$ is the characteristic relaxation time in this equation, $\Delta\varepsilon(T,P) = \varepsilon_o(T,P) - \varepsilon_\infty(T,P)$ is the relaxation strength, m, n (with limits $0 < m$, $mn \leq 1$) describe, respectively, the symmetrical and asymmetrical broadening of the distribution of relaxation times, σ_o is the dc-conductivity, and ε_f is the permittivity of free space. From τ_{HN}, the relaxation time at maximum loss, τ_{max}, is obtained analytically following[32]

$$\tau_{max} = \tau_{HN}\left[\frac{\sin\left(\frac{\pi m}{2+2n}\right)}{\sin\left(\frac{\pi mn}{2+2n}\right)}\right]^{-1/m} \quad (2)$$

At high temperatures, the derivative of ε' $(d\varepsilon'/d\ln\omega \approx -(2/\pi)\varepsilon'')$ has been used in order to avoid the conductivity contribution.[33]

Pressure−Volume−Temperature Measurements (PVT). The PVT measurements on the $PS_{28}/PMPS_{17}$ blend were made by A. Best (MPI-P, Mainz) with a Gnomix dilatometer using the confining fluid technique (mercury). Measurements were made under "isobaric" conditions within the temperature range from 303 to 423 K and for pressures in the range from 10 to 200 MPa (see Figure S1 in the Supporting Information).

3. Results and Discussion

We first briefly discuss the results for the $PS_{48}/PMPS_{17}$ blend which is expected to be in the phase-separated state for reasons which are discussed below. The dielectric loss spectra in Figure 1 display two processes ("fast" and "slow"), and thus a summation of two HN functions was employed and some representative fits are included in the figure.

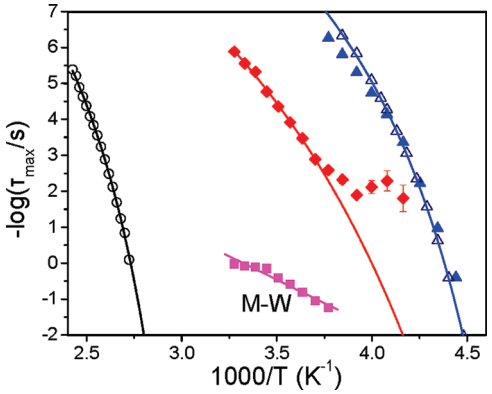

Figure 2. Arrhenius relaxation map of the relaxation processes in the $PS_{48}/PMPS_{17}$ blend and the corresponding homopolymers (open symbols); (circles) PS; (triangles) PMPS; (filled rhombus) "slow" process in the blend; (filled triangles) "fast" process in the blend. Solid lines are fits to the VFT equation (see text).

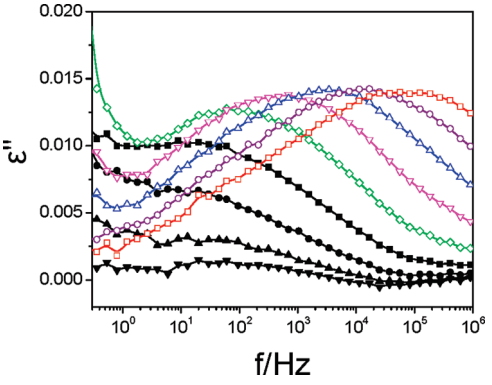

Figure 3. Dielectric loss curves for the $PS_{28}/PMPS_{17}$ blend at different temperatures: (open squares) 285.15; (open circles) 279.15; (open up triangles) 273.15; (open down triangles) 267.15 K; (open rhombus) 261.15; (filled squares) 255.15; (filled circles) 249.15; (filled triangles) 243.15; and (filled down triangles) 237.15 K. The curves are asymmetrically broadened toward low frequencies. Notice that at $T < 255.15$ K, the main process loses intensity.

The two processes have the following HN shape parameters: $m = 0.50 \pm 0.05$, $n = 1$ for the "fast" and $m = 0.22 \pm 0.01$, $n = 1$ for the slower component, suggesting a very broad distribution of relaxation times for the latter process (the corresponding homopolymer values are $m = 0.81 \pm 0.04$, $n = 0.48 \pm 0.03$ and $m = 0.65 \pm 0.05$, $n = 0.39 \pm 0.05$ for PMPS and PS, respectively).

The relaxation times, depicted in Figure 2 at $P = 0.1$ MPa, display the usual Vogel−Fulcher−Tammann (VFT) temperature dependence

$$\tau_{max} = \tau_0 \exp \frac{B}{T - T_0} \tag{3}$$

where T_0 is the "ideal" glass temperature, τ_0 is the characteristic time in the limit of very high temperatures, and B is the activation parameter with values: $\tau_0 = 2 \times 10^{-14}$ and 2×10^{-15} s; $B = 2260$ and 1408 K; and $T_0 = 294$ and 186.7 K for the PS and PMPS homopolymers, respectively. The corresponding values for the "fast" process are: $\tau_0 = 2 \times 10^{-13}$ s, $B = 1130$ K, and $T_0 = 188$ K, whereas for the "slower" process within a limited temperature range, $\tau_0 = 2 \times 10^{-15}$ s, $B = 2770$ K, and $T_0 = 168$ K. The proximity of the "fast" process in the blend to the bulk PMPS segmental dynamics as well as the presence of an even slower process due to the Maxwell−Wagner polarization of inhomogeneous media[32] (with shape parameters $m = 0.8$, $n = 1.0$ and an activation energy of 59 ± 3 kJ/mol) is a clear indication of phase separation and this is in agreement with the spinodal temperature for this blend ($T \approx 370$ K, the theoretically predicted phase diagram for this blend is shown in Figure S3 of the Supporting Information).

We can further employ the dielectric strength of the "fast" process (or better the value of the product $T\Delta\varepsilon^{fast} \approx 20$ K, which takes into account the weak T-dependence of $\Delta\varepsilon$) as compared to the homopolymer values ($T\Delta\varepsilon^{PS} \approx 20$ K, $T\Delta\varepsilon^{PMPS} \approx 80$ K) to obtain an estimate of the composition of phases as

$$\Delta\varepsilon_{PMPS}{}^{PMPS\text{-}rich} = w^{PMPS} \varphi_{PMPS}{}^{PMPS\text{-}rich} \Delta\varepsilon_{PMPS}{}^{0} \tag{4}$$

where $\Delta\varepsilon_{PMPS}{}^{PMPS\text{-}rich}$ and $\varphi_{PMPS}{}^{PMPS\text{-}rich}$ are, respectively, the dielectric strength and composition of PMPS in the PMPS-rich phase, $\Delta\varepsilon_{PMPS}{}^{0}$ is the dielectric strength of bulk PMPS, and w^{PMPS} is the mass fraction of the mixture in the PMPS phase ($w^{PMPS} + w^{PS} = 1$). The latter is given by the lever rule $w^{PMPS} = (\varphi_{PS}{}^{PS\text{-}rich} - \langle\varphi\rangle)/(\varphi_{PS}{}^{PS\text{-}rich} - \varphi_{PS}{}^{PMPS\text{-}rich})$ where $\langle\varphi\rangle$ is the average blend composition. Under the assumption of a pure mobile phase (i.e., $\varphi_{PMPS}{}^{PMPS\text{-}rich} \approx 1$) that is justified by the close proximity of the "fast" process to the bulk PMPS segmental dynamics, eq 4 results in $\varphi_{PS}{}^{PS\text{-}rich} = 0.67$. The latter value, being ≪1, can be understood by the interplay between spinodal decomposition and glass transition; quenching into the unstable region gives rise to phase separation by spinodal decomposition, but the phase separation is distinctly different than in a mixture of liquids. Although the mixture rich in the soft component (PMPS) attains its equilibrium composition, this is not the case with the mixture rich in the glassy component (PS). For the latter, the domain growth is gradually frozen before the equilibrium concentration can be reached. This effectively gives rise to an enriched PMPS component in the mixture containing a majority of the glassy phase.[29] Thus, the dielectric strength of the "slower" process may reflect the PMPS and PS segmental relaxations within the PS-rich phase. A coarsening mechanism has been proposed[34] that involves the migration and coalescence of liquid PMPS droplets within the glassy PS matrix that could be responsible for the very broad distribution of relaxation times associated with the "slower" process. Thus the segmental dynamics for the $PS_{48}/PMPS_{17}$ blend comply with the dynamics of phase-separated blends with a glassy component.

The segmental dynamics in the lower molecular weight blend (that was optically clear at room temperature) were completely altered and deserve more attention. The dielectric loss curves in the $PS_{28}/PMPS_{17}$ blend are shown in Figure 3 and display asymmetric broadening toward lower frequencies.

A single Havriliak−Negami function can not capture this asymmetry. Therefore a summation of two HN functions was employed and a representative fit is shown in Figure 4. The figure depicts a "fast" and a "slow" process with separation that depends on temperature (see below).

The corresponding "slow" and "fast" relaxation times are shown in Figure 5 at $P = 0.1$ MPa as a function of temperature together with the homopolymer segmental dynamics (depicted with open symbols). All display the usual VFT temperature dependence.

Notice that the "slower" process in the blend approaches the faster one with decreasing temperature. This $\tau(T)$ for the slower process is peculiar and is uncommon for miscible polymer blends, as we will see below in detail. In addition, below about 255 K, the dielectric strength of the faster processes is dramatically reduced (Figure 3) and the associated dynamics become weakly dependent on temperature. The latter may reflect the confinement effects on the faster process by the slower moving species.[21]

In an effort to account for the two relaxation processes in the blend, we first employ the "self-concentration" model of Lodge and McLeish (LM) describing the segmental dynamics in miscible blends.[10] According to the model, the average composition of the local environment around any chosen segment is enriched in the

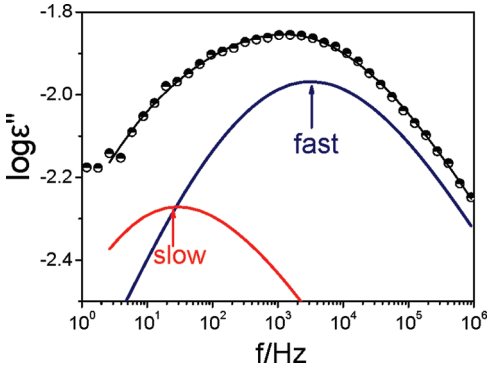

Figure 4. Analysis of the dielectric loss at 270.15 K by two Havriliak−Negami functions indicated as "fast" and "slow".

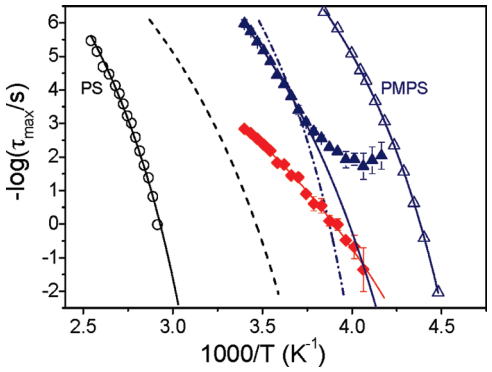

Figure 5. Arrhenius relaxation map of the relaxation processes in the $PS_{28}/PMPS_{17}$ blend and the corresponding homopolymers (open symbols); (circles) PS; (triangles) PMPS; (filled rhombus) "slow" process in the blend; (filled triangles) "fast" process in the blend. Solid lines are fits to the VFT equation. Dashed and dash-dotted lines are the predictions of the LM model for the PS and PMPS segmental dynamics in the blend.

same species because of chain connectivity effects. Because of this, each species will experience a different average local environment and to the extent that the glass transition is sensitive to composition, each polymer will sense its own composition-dependent glass temperature. In a binary blend of homopolymers A and B, the effective local concentration is defined by

$$\varphi_{\mathrm{eff},i} = \varphi_{S,i} + (1-\varphi_{\mathrm{S},i})\langle\varphi\rangle \tag{5}$$

where i represents component A or B, and φ_S is the self-concentration. According to the LM model, the relevant length scale in evaluating the self-concentration, is the Kuhn length (l_K) of the polymer. The model describes reasonably well the segmental dynamics of miscible blends both as a function of temperature and pressure. The self-concentration is determined from the volume fraction occupied by monomers in one Kuhn length inside a volume $V = l_K^3$ as

$$\varphi_S = \frac{C_\infty M_0}{k\rho N_A V_K} \tag{6}$$

where C_∞ is the characteristic ratio, M_0 is the repeat unit molar mass, N_A is Avogadro's number, and k is the number of backbone bonds per repeat unit. The model associates the average local concentration of each component with a local glass temperature

$$T_{g,\mathrm{eff}} = T_g(\varphi)|_{\varphi=\varphi_{\mathrm{eff}}} \tag{7}$$

Hence the effective glass temperature, $T_{g,\mathrm{eff}}$, is determined from the macroscopic $T_g(\varphi)$ but evaluated at φ_{eff} rather than φ. For the

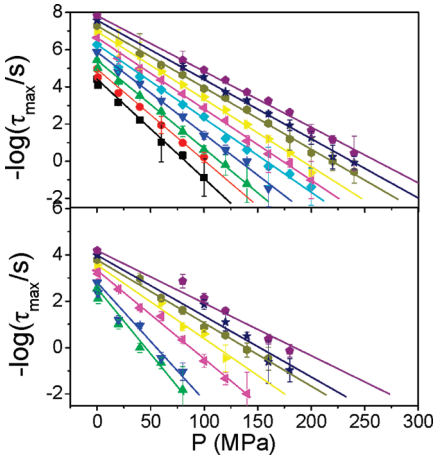

Figure 6. Pressure dependence of the "fast" (top) and "slow" (bottom) processes in the $PS_{28}/PMPS_{17}$ blend at different temperatures: (squares) 278.15; (circles) 283.15; (up triangles) 288.15; (down triangles) 293.15; (rhombus) 298.15; (left triangles) 303.15; (right triangles) 308.15; (polygon) 313.15; (star) 318.15; (pentagon) 323.15 K. The lines represent the result of linear fits to the data (forced to the $P = 0.1$ MPa data).

macroscopic composition dependence of the glass temperature the well-known Fox equation was assumed but with the effective concentration for each component instead of the total blend composition $\langle\varphi\rangle$ as:

$$\frac{1}{T_g(\varphi)} = \frac{\varphi_A}{T_{g,A}} + \frac{1-\varphi_A}{T_{g,B}} \tag{8}$$

To test the model predictions against the full $\tau(T)$ dependence at 0.1 MPa the following parameters were employed: $C_\infty = 9.5$, $M_0 = 0.104$ kg/mol, $k = 2$, $\rho = 1050$ kg/m^3, $l_K = 1.47$ nm resulting in $\varphi_S = 0.25$ for PS and $C_\infty = 8.8$, $M_0 = 0.136$ kg/mol, $k = 2$, $\rho = 1118$ kg/m^3, $l_K = 1.43$ nm, and $\varphi_S = 0.30$ for PMPS. For the segmental dynamics in the blends we have further assumed

$$\tau_i(\varphi_{\mathrm{eff}}, T) = \tau_{0,i}\exp\left(\frac{B_i}{T - T_{0,i}(\varphi_{\mathrm{eff}})}\right) \tag{9}$$

with identical B_i and $\tau_{0,i}$ parameters as for bulk PS and PMPS, where only the ideal glass temperature varies with composition, and

$$T_{0,i}(\varphi_{\mathrm{eff}}) = T_{0,i} + [T_{g,i}(\varphi_{\mathrm{eff}}) - T_{g,i}] \tag{10}$$

where $T_{0,i}$ is the ideal glass temperature for homopolymers A or B and $T_{0,i}(\varphi_{\mathrm{eff}})$ is the ideal glass temperature for each component in the blend. The thus obtained predictions of the LM model for the PS and PMPS segmental relaxations in the $PS_{28}/PMPS_{17}$ blend are shown in Figure 5 with the dashed (PS) and dash-dotted (PMPS) lines. Although the "fast" process is reasonably described by the model, the "slow" mode can not be predicted (shown with the dashed line) and this despite the fact that the LM model predicts reasonably well the dynamics of the high T_g component in miscible blends.[18]

The inability of the model to account for the slower process as well as the peculiar $\tau(T)$ dependence for this process could suggest phase separation. We further propose at this point that the "slow" and "fast" processes in the blend reflect the PMPS segmental dynamics in PS-rich and PMPS-rich domains. There are experiments that can test this hypothesis. One such experiment is through the application of pressure and is based on the different pressure sensitivity of the segmental relaxations of different polymers. The pressure sensitivity can be parametrized through the apparent activation volume, defined as $\Delta V^{\#} = RT(\partial \ln \tau/\partial P)_T$.[19] Figure 6 shows the pressure dependence of the "slow" and "fast"

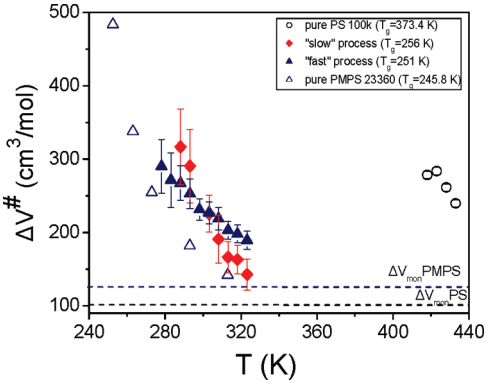

Figure 7. Apparent activation volume, $\Delta V^{\#}$, for the "fast" (filled triangles) and "slow" (filled rhombus) processes in the $PS_{28}/PMPS_{17}$ blend compared to PMPS homopolymer (open triangles)[36] and PS homopolymer (open circles).[37] Notice the proximity of the values for the "slow" and "fast" processes to the bulk PMPS values. Dashed horizontal lines give the monomer volumes of PMPS (blue) and PS (black).

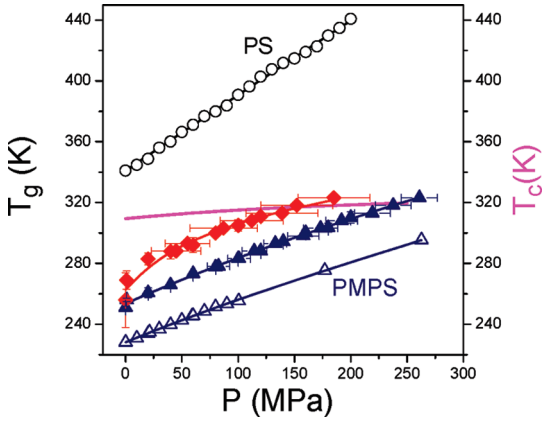

Figure 8. Pressure dependence of T_g (defined at $\tau \approx 1$ s) for the "fast" (filled triangles) the "slow" (filled rhombus) processes in the $PS_{28}/PMPS_{17}$ blend and of the PMPS (open triangles, ref 36) and PS (open circles, T_g-scaled data from ref 38) homopolymers. Notice the proximity of the two T_g values at all pressures investigated. The solid line (magenta) is the $T_c(P)$ theoretical prediction.

modes and Figure 7 gives the calculated apparent activation volumes.

The effect of pressure is to slow the segmental dynamics through densification, but the extent of this effect depends largely on temperature and the polymer involved. We have shown that $\Delta V^{\#}$ is strongly temperature dependent near T_g and approaches the monomer volume at $T_g + 100$ K.[35] As can be seen in Figure 7, both the "slow" and "fast" process have $\Delta V^{\#}$ values in the vicinity of bulk PMPS, thus confirming the assignment as reflecting PMPS segmental relaxations (in PS- and PMPS-rich domains). In fact, the slower process shows a somewhat steeper T-dependence, reflecting a contribution from the PS-rich environment to the PMPS relaxation.

A second experiment is through the pressure sensitivity of the glass temperature. In Figure 8 the $T_g(P)$ dependencies of the "slow" and "fast" components in the blend extracted from the "isothermal" (Figure 7) and "isobaric" (not shown) data are plotted. In the same plot we include the model prediction for $T_c(P)$ that will be discussed latter. The $T_g(P)$ can be described according to the empirical equation:

$$T_g(P) = T_g(0)\left(1+\frac{\kappa}{\lambda}P\right)^{1/\kappa} \qquad (11)$$

where $T_g(0)$ is the temperature where the characteristic relaxation time of each process corresponds to 1 s, and κ, λ are polymer specific parameters that are summarized in Table 3 together with the initial slopes, $(dT/dP)_{P\to 0}$.

Notice the similar $T_g(P)$ dependence for the two modes in the blend as with the bulk PMPS and that can be distinguished from the steeper $T_g(P)$ dependence of bulk PS (also included in the figure). This is also shown by the proximity of the pressure coefficients of the "fast" process to the PMPS homopolymer value. The corresponding value for the "slower" process is unreasonably high, which could reflect some contribution by PS within an initial pressure range.

We can reinforce the experimental evidence above using modeling calculations which aim to predict the phase behavior of the $PS_{28}/PMPS_{17}$ system directly. Here we will show that these results do indeed indicate phase separation in the range of the experimental measurements. In these calculations, we have employed a theoretical lattice-based equation of state for chain-molecule fluids.[28,39,40] In contrast to Flory–Huggins theory,[41] the present theory accounts for both the effects of compressibility and nonrandom mixing. Briefly, the derivation employs an athermal reference state along with an integral equation formalism to

Table 3. Parameters of eq 11 and Initial Slopes $(dT/dP)_{P\to 0}$ for the $PS_{28}/PMPS_{17}$ Blend and the Respective Homopolymers

process	$T_g(0)$ (K) (τ = 1 s)	κ	λ (MPa)	$(dT/dP)_{P\to 0}$ (K/MPa)
PS	341	1.1 ± 0.1	680 ± 15	0.50 ± 0.01
"slow"	256	10.3 ± 1.7	270 ± 60	0.9 ± 0.3
"fast"	251	2.6 ± 0.3	770 ± 30	0.32 ± 0.02
PMPS	228	2.2 ± 0.1	760 ± 10	0.30 ± 0.01

determine the nearest neighbor probabilities, for all possible neighboring pairs, at finite temperature. These probabilities lead to the calculation of the system's internal energy and, ultimately, produce a closed-form expression for the Helmholtz free energy. The resulting equation of state is expressed in terms of a set of transferable microscopic parameters. This means that these parameters can be determined by fitting to a limited set of experimental data on known physical properties, and then used to predict other properties.

As an example of the equation of state, we show here the pressure of a pure chain fluid as a function of the number of chain molecules (N), volume (V), and temperature (T)

$$\frac{P}{k_B T} = \left(\frac{1}{v}\right)\ln\left(\frac{V}{V-rvN}\right) + \left(\frac{z}{2v}\right)\ln\left(\frac{V-(2vN/z)(r-1)}{V}\right) - \left(\frac{z}{2v}\right)\left(\frac{r-(2/z)(r-1)}{(V/vN)-(2/z)(r-1)}\right) \times \left\{\frac{[r-(2/z)(r-1)](\exp[-u/k_B T]-1)}{[r-(2/z)(r-1)]\exp[-u/k_B T]+(V/vN)-r}\right\} \qquad (12)$$

In this equation, the key microscopic parameters are v, the volume per lattice site; u, the nearest neighbor segment–segment interaction energy,[42] and r, the number of segments per molecule (z is the lattice coordination number ,which is always fixed at a value of 6[43]). It is noted that the compressible nature of the fluid is reflected in the fact that V (in eq 12) comprises contributions from both filled and empty lattice sites. For the case of binary mixtures (blends), the equation of state follows a similar form wherein three additional parameters are incorporated. Specifically, there is r and u for the second component, and the parameter, g, which scales the mixed energetic interaction (u_{ab}) according to $u_{ab} = g(u_{aa}u_{bb})^{1/2}$. Note that the lattice mixtures are modeled using a single value for v, which is chosen to be a compromise for the two components. Finally, it is important to point out that, for polymers, once the r parameter has been fit to one molecular

Table 4. Parameter Set for the Theoretical Equation of State[a]

	r/M (g/mol)$^{-1}$	$-u$ (J/mol)	v (mL/mol)	g
PS	0.109697	2104.46	8.000	0.997592
PMPS	0.105732	2056.37		

[a] r is the number of lattice sites per chain molecule; v is the volume per lattice site; u is the interaction energy between the sites; g scales the mixed interaction energy according to $u_{ab} = g(u_{aa}u_{bb})^{1/2}$.; M is the molecular weight.

weight, it can then be readily scaled (with the other parameters fixed) to predict the properties for other molecular weights. That is, the appropriate r for any predicted system, "$r_{predict}$", would be given by $r_{predict} = M_{predict}(r_{fit}/M_{fit})$; this property is used frequently and thus we tabulate the r parameter as r/M. In addition, the theory correctly predicts the experimentally observed increase in compressibility with lowering molecular weight.

The parameters, r, v, and u for each component are typically determined from the pure fluid pressure−volume−temperature (PVT) data (when available for each pure component). In this work, we obtained the PS parameters by fitting to pure PS PVT data,[38] and (using these PS parameters) we then fit the PMPS parameters to the available set of PS/PMPS mixed system PVT data (assuming $g = 1$; see the discussion below). A more detailed description of the fitting procedure is available in Supporting Information. The resulting PS and PMPS parameters are summarized in Table 4, and examples of $V(T)$ curves at low pressure for each pure component and for the PS/PMPS blend are given in the lower panel of Figure 9; the PS and PS/PMPS curves are fits, the curve for pure PMPS is thus a prediction.

The one remaining parameter, g, cannot be determined from pure component data, or, in general, from mixed system PVT data. This is because g does not strongly influence PVT properties over its range of typical values (which are always extremely close to unity). On the other hand, properties related to the second derivative of the free energy are quite sensitive to g. One option is thus to utilize an experimental critical temperature, for example, an upper or lower critical solution temperature ("UCST" or "LCST"). Here, by changing g with the other parameters fixed, the theoretical critical temperature is fit to the experimental value. (The remainder of the theoretical phase diagram thus comprises a true "prediction".) Upon obtaining a value for g, other predictions are then possible, such as phase diagrams for related systems of different molecular weights (e.g., by scaling r) or phase behavior at other pressures, as well as the various thermodynamic mixing functions.

To fit g, we employ the cloud point data from ref 44. In that work, an experimental PS/PMPS system having molecular weights of 6682 [PS] and 2271 [PMPS] was shown to exhibit UCST-type phase separation with a critical temperature of ~390 K. It is noted that the presently studied $PS_{28}/PMPS_{17}$ system ($M_w = 2940$ [PS] and 2347 [PMPS]) has significantly lower molecular weight (for PS) and thus should still be potentially miscible below this temperature (390 K).

The theoretical fit to the experimental cloud point data is given in the upper panel of Figure 9. The fact that the present theory is able to predict the UCST-type phase behavior is noteworthy. In ref 44, modeling calculations were unsuccessfully attempted using two other theories (lattice fluid theory[45,46] and an EOS due to Patterson[47]). In both cases, the theoretical PS/PMPS phase diagrams had an incorrect form, showing both UCST and, LCST-type phase boundaries. Furthermore, when attempts were made to fit the UCST to the experimental value, the boundaries merged into an hourglass diagram (i.e., two phases at all temperatures).

Our complete set of parameters (Table 4) allows us to predict the phase behavior for the present $PS_{28}/PMPS_{17}$ system. As mentioned above, we expect the onset of partial miscibility for

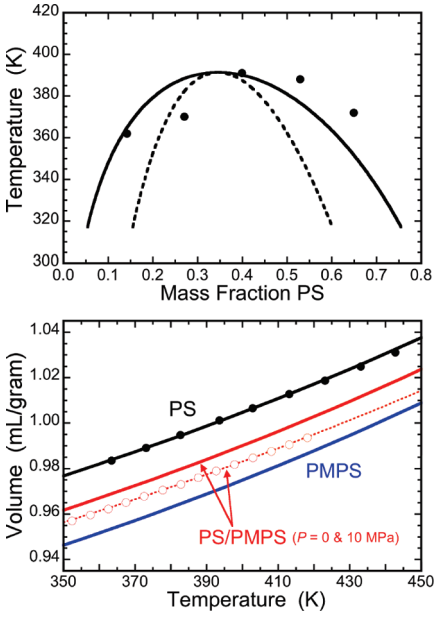

Figure 9. Fitting results for the model equation of state. Given in the lower panel are the $V(T)$ curves at atmospheric pressure (solid curves) for PS ($M_w = 9000$ g/mol), PMPS ($M_w = 2347$), and the PS/PMPS blend ($M_w = 2940$ (PS) and 2347 (PMPS), i.e., $PS_{28}/PMPS_{17}$). Also given is $V(T)$ at 10 MPa for the PS/PMPS blend (dashed curve). The symbols represent experimental data; the PS data is from ref 36; the PS/PMPS data, for 10 MPa and above, are described in the Supporting Information (only every fifth point is shown here for clarity). The pure PMPS curve is predicted from the fit to the PS/PMPS blend data. Given in the upper panel is the model phase diagram corresponding to the experimental PS/PMPS blend studied in ref 44 with molecular weights (M_w) of 6682 (PS) and 2271 (PMPS). One model parameter (g) has been fit to match the experimental critical temperature. The binodal is given by the solid curve and the spinodal by the dashed curve. The symbols are the experimental cloud point data.

this system to lie somewhere below a temperature of 390 K. In particular, we are interested in the phase behavior in the temperature range of the experimental DS measurements (T ranging from ~235 to 295 K, at atmospheric pressure and an overall $\varphi_{PS} = 0.5$). For a temperature of 260 K, we first show in Figure 10 the theoretical prediction for the Gibbs free energy of mixing (ΔG_{mix}) as a function of composition (at atmospheric pressure (0.1 MPa)). The predicted curve clearly shows two points of inflection indicating the presence of two phases. The complete phase diagram for $PS_{28}/PMPS_{17}$ is shown in Figure 11. The phase boundary terminates at a predicted UCST of 309 K,[48] and thus, the theory predicts two-phase behavior over the entire temperature range of the DS measurements.

On the basis of the calculated binodals (spinodals), the compositions of each phase at say, 260 K, are as follows: $\varphi_{PS}^{PMPS\text{-rich}} = 0.13$ (0.25) ($\varphi_{PMPS}^{PMPS\text{-rich}} = 0.87$ (0.75)) and $\varphi_{PS}^{PS\text{-rich}} = 0.80$ (0.66) ($\varphi_{PMPS}^{PS\text{-rich}} = 0.20$ (0.34)). (These values can be verified as the double-tangent and inflection points of ΔG_{mix} in figure 10.) We can test these compositions against the experimental data for the dielectric strengths of the "fast" and "slow" processes (with respective values of $T\Delta\varepsilon \approx 30$ and 10 K). Using a generalized equation that accounts for the PS contribution within the "fast" process (due to incomplete phase separation) as

$$\Delta\varepsilon^{PMPS\text{-rich}} = w^{PMPS}(\varphi_{PS}^{PMPS\text{-rich}}\Delta\varepsilon_{PS}^{0} + \varphi_{PMPS}^{PMPS\text{-rich}}\Delta\varepsilon_{PMPS}^{0}) \quad (13)$$

gives $T\Delta\varepsilon \approx 32.3$ K (25.4 K), in excellent agreement with the intensity of the "fast" process. We should point out, however, that the second term accounts for 96% (92%) of the total intensity

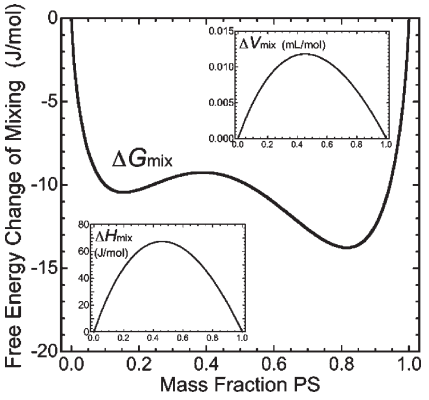

Figure 10. Model predictions for the thermodynamic mixing functions at 260 K and atmospheric pressure. Given here is the Gibbs free energy of mixing (ΔG_{mix}) as a function of composition for the $PS_{28}/PMPS_{17}$ system. Included in the insets are the corresponding enthalpy and volume changes on mixing (ΔH_{mix} and ΔV_{mix}). ΔG_{mix} and ΔH_{mix} are given in units of Joules per mole of repeat units, and ΔV_{mix} is in units of milliters per mole of repeat units.

within the PMPS-rich phase. As for the slower component, the estimated strength within the PS-rich phase is $\Delta\varepsilon_{PMPS}^{PS\text{-}rich} = w^{PS}\varphi_{PMPS}^{PS\text{-}rich}\Delta\varepsilon_{PMPS}^{o} \approx 8.8$ K (16.6 K), i.e., in excellent agreement with the intensity of the "slower" process. Thus the two processes reflect PMPS dynamics in PMPS- and PS-rich environments.

The modeling results discussed so far correspond to predictions for the phase behavior at atmospheric pressure. Given that some of the key experimental evidence for phase separation has involved probing the pressure dependence of the dielectrically active segmental dynamics, it is of interest to also investigate the model predictions for the phase behavior at elevated pressures. Particularly relevant is the pressure dependence of the critical temperature in relation to the $T_g(P)$ dependence of the two processes in the blend. The slope of $T_c(P)$ can be conveniently estimated using the approximate expression[49]

$$\frac{dT_c}{dP} \approx T_c \frac{\Delta V_{mix}^c}{\Delta H_{mix}^c} \quad (14)$$

where ΔV_{mix}^c and ΔH_{mix}^c are the volume and enthalpy changes on mixing evaluated at the critical point, and where T_c could imply, in general, a UCST or LCST. (This expression relies on the assumption that ΔV_{mix} and ΔH_{mix} have similar functional form, allowing one to replace the exact expression involving the ratio of the second derivatives of these quantities.[49]) An increase in pressure for LCST-type polymer blends always increases the miscibility (raises the LCST) because ΔV_{mix} and ΔH_{mix} are both always negative. For a UCST-type system, on the other hand, an increase in P could shift the UCST in either direction because (depending on the particular system) there could be either a positive or negative ΔV_{mix} (with $\Delta H_{mix} > 0$).

Shown in the insets of Figure 10 are ΔV_{mix} and ΔH_{mix} as a function of composition at a temperature of 260 K and atmospheric pressure (same as for ΔG_{mix}). As expected for UCST-type blends, ΔH_{mix} is positive, and the theory further predicts a positive ΔV_{mix} ($\Delta V_{mix}/V \approx 1.1 \times 10^{-4}$ at $\varphi_{PS} = 0.5$). The general trends in ΔV_{mix} and ΔH_{mix} are fairly similar at the critical temperature (here ΔV_{mix} is roughly 40% larger), and thus eq 14 indicates that the UCST will increase (modestly) with pressure. Explicit model predictions for the UCST as a function of P are shown in Figure 8, and indeed the critical temperature is seen to increase (by ~11 K) upon increasing the pressure to 250 MPa (from 309 to 320 K). Again (as seen in the figure), the model calculations show that the $PS_{28}/PMPS_{17}$ system is phase-separated

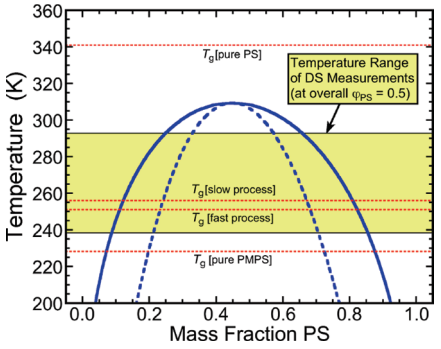

Figure 11. Predicted phase diagram for $PS_{28}/PMPS_{17}$ at atmospheric pressure. Given are the binodal (solid) and spinodal (dashed) curves. The shaded region indicates the temperature range of the DS measurements (all performed at a single overall blend composition of $\varphi_{PS} = 0.5$). Also marked (by dashed lines) are the glass temperatures (defined by $\tau = 1$ s) for the fast and slow processes as well as those for pure PS and PMPS.

over nearly the entire range of the DS measurements at elevated pressures. Because of the different pressure dependencies of the critical temperature ($dT_c/dP \approx 0.07$ K/MPa) and of the glass temperatures corresponding to the PMPS segmental dynamics (Table 3), the prediction is that the blend will become thermodynamically homogeneous above about 250−300 MPa (i.e., within a range that is in the limit of our experimental window). Nevertheless, the model predictions confirmed the presence of phase-separated domains in the $PS_{28}/PMPS_{17}$ blend that allow understanding of the peculiar dynamics in terms of PMPS segmental relaxation in two different environments.

4. Conclusions

The segmental dynamics in two symmetric blends of PMPS and PS were studied as a function of temperature and pressure. The dynamics in the high molecular weight blend were reminiscent of phase-separated blends with one glassy component, where the interplay between spinodal decomposition and glass transition results in the enrichment of the high T_g component by the more mobile component. To identify the origin of the complex dynamics in the lower-molecular-weight blend, the temperature- and pressure-dependent studies were coupled with model calculations of the phase behavior as a function of the thermodynamic variables. The distinctly different pressure sensitivity of PS and PMPS allowed identifying the origin of the two dynamic processes as reflecting the PMPS segmental dynamics in PMPS-rich and PS-rich domains. Model calculations using a lattice-based equation of state allowed for prediction of the phase diagram and the effect of pressure on the critical temperature for the same blend. The pressure coefficient of the critical temperature (dT_c/dP) was only a fraction of the corresponding coefficient of the glass temperatures suggesting that a transition to a thermodynamically miscible but dynamically heterogeneous state will take place for pressures above 300 MPa.

Acknowledgment. G.F. thanks Mr. A. Best at the MPI-P for the PVT measurements and Mr. G. Tsoumanis (UoI) for technical support. This research project (PENED856) is cofinanced by E.U.-European Social Fund (80%) and the Greek Ministry of Development-GSRT (20%). J.E.G.L. and R.P.W. gratefully acknowledge financial support by the National Science Foundation (Grants DMR-0502196 and DMR-0804593).

Supporting Information Available: Additional information, figures, and tables (PDF). This material is available free of charge via the Internet at http://pubs.acs.org.

References and Notes

(1) Colby, R. H. *Polymer* **1989**, *30*, 1275.
(2) Miller, J. B.; McGrath, K. J.; Roland, C. M.; Trask, C. A.; Garroway, A. N. *Macromolecules* **1990**, *23*, 4543.
(3) Chin, Y. H.; Zhang, C.; Wang, P.; Inglefield, P. T.; Jones, A. A.; Kambour, R. P.; Bendler, J. T.; White, D. M. *Macromolecules* **1992**, *25*, 3031.
(4) Roland, C. M.; Ngai, K. L. *Macromolecules* **1991**, *24*, 2261.
(5) Pathak, J. A.; Colby, R. H.; Floudas, G.; Jerome, R. *Macromolecules* **1999**, *32*, 2553.
(6) He, Y.; Lutz, T. R.; Ediger, M. D. *J. Chem. Phys.* **2003**, *119*, 9956.
(7) Krygier, E.; Lin, G.; Mendes, J.; Mukandela, G.; Azar, D.; Jones, A. A.; Pathak, J. A.; Colby, R. H.; Kumar, S. K.; Floudas, G.; Krishnamoutri, R.; Faust, R. *Macromolecules* **2005**, *38*, 7721.
(8) Pathak, J. A.; Colby, R. H.; Kamath, S. Y.; Kumar, S. K.; Stadler, R. *Macromolecules* **1998**, *31*, 8988.
(9) Zetsche, A.; Fischer, E. W. *Acta Polym.* **1994**, *45*, 168.
(10) Lodge, T. P.; McLeish, T. C. B. *Macromolecules* **2000**, *33*, 5278.
(11) Chung, G.-C.; Kornfield, J. A.; Smith, S. D. *Macromolecules* **1994**, *27*, 964.
(12) Kant, R.; Kumar, S. K.; Colby, R. H. *Macromolecules* **2003**, *36*, 10087.
(13) Kamath, S.; Colby, R. H.; Kumar, S. K.; Karatasos, K.; Floudas, G.; Fytas, G.; Roovers, J. E. L. *J. Chem. Phys.* **1999**, *111*, 6121.
(14) Kumar, S. K.; Colby, R. H.; Anastasiadis, S. H.; Fytas, G. *J. Chem. Phys.* **1996**, *105*, 3777.
(15) Cangialosi, D.; Alegria, A.; Colmenero, J. *Macromolecules* **2006**, *39*, 7149.
(16) Colby, R. H.; Lipson, J. E. G. *Macromolecules* **2005**, *38*, 4919.
(17) Floudas, G.; Fytas, G.; Reisinger, T.; Wegner, G. *J. Chem. Phys.* **1999**, *111*, 9129.
(18) Mpoukouvalas, K.; Floudas, G. *Macromolecules* **2008**, *41*, 1552.
(19) Floudas, G. In *Broadband Dielectric Spectroscopy*; Kremer, F., Schönhals, A. Eds.; Springer: Berlin, 2002; Chapter 8.
(20) Alegria, A.; Gomez, D.; Colmenero, J. *Macromolecules* **2002**, *35*, 2030.
(21) Schwartz, G. A.; Colmenero, J.; Alegria, A. *Macromolecules* **2007**, *40*, 3246.
(22) Schwartz, G. A.; Alegria, A.; Colmenero, J. *J. Chem. Phys.* **2007**, *127*, 154907.
(23) Roland, C. M.; Casalini, R. *Macromolecules* **2007**, *40*, 3631.
(24) Mpoukouvalas, K.; Floudas, G.; Zhang, S. H.; Runt, J. *Macromolecules* **2005**, *38*, 552.
(25) Zhang, S. H.; Casalini, R.; Runt, J.; Roland, C. M. *Macromolecules* **2003**, *36*, 9917.
(26) Mpoukouvalas, K.; Floudas, G.; Verdock, B.; Du Prez, F. E. *Phys. Rev. E* **2005**, *72*, 011802.
(27) Kumar, S. K. *Macromolecules* **2000**, *33*, 5285.
(28) Lipson, J. E. G.; Tambasco, M.; Willets, K. A.; Higgins, J. S. *Macromolecules* **2003**, *36*, 2977.
(29) Karatasos, K.; Vlachos, G.; Vlassopoulos, D.; Fytas, G.; Meier, G.; Du Chesne, A. *J. Chem. Phys.* **1998**, *108*, 5997.
(30) Vlassopoulos, D.; Koumoutsakos, A.; Anastasiadis, S. H.; Hatzikiriakos, S. G.; Englezos, P. *J. Rheol.* **1997**, *41*, 739.
(31) Havriliak, S.; Negami, S. *Polymer* **1967**, *8*, 161.
(32) Kremer, F.; Schoenhals, A., Eds. *Broadband Dielectric Spectroscopy*; Springer: Berlin, 2002.
(33) Steeman, P. A. M.; van Turnhout, J. *Macromolecules* **1994**, *27*, 5421.
(34) Sappelt, D.; Jäckle, J. *Physica A* **1997**, *240*, 453.
(35) Floudas, G.; Gravalidis, C.; Reisinger, T.; Wegner, G. *J. Chem. Phys.* **1999**, *111*, 9847.
(36) Paluch, M.; Casalini, R.; Patkowski, A.; Pakula, T.; Roland, C. M. *Phys. Rev. E* **2003**, *68*, 031802.
(37) The apparent activation volume of PS is from ref 19 and corresponds to a high-molecular-weight homopolymer ($M_w = 1 \times 10^5$ g/mol).
(38) Zoller, P.; Walsh, D. *Pressure−Volume−Temperature Data for Polymers*; Technomic Publishing Co.: Lancaster, PA, 1995.
(39) Lipson, J. E. G. *Macromol. Theory Simul.* **1998**, *7*, 263.
(40) Tambasco, M.; Lipson, J. E. G.; Higgins, J. S. *Macromolecules* **2006**, *39*, 4860.
(41) Flory, P. J. *Principles of Polymer Chemistry*; Cornell University Press: Ithaca, NY, 1956.
(42) In other work, the nearest neighbor interaction energy has usually been denoted by ε.
(43) Changing the value of z will change the values of the other parameters, but it does not change the overall quality of the fitted physical properties.
(44) Rudolf, B.; Cantow, H.-J. *Macromolecules* **1995**, *28*, 6586.
(45) Sanchez, I. C.; Lacombe, R. H. *J. Phys. Chem.* **1976**, *80*, 2352.
(46) Lacombe, R. H.; Sanchez, I. C. *J. Phys. Chem.* **1976**, *80*, 2568.
(47) Patterson, D. *J. Polym. Sci., Part C* **1968**, *16*, 3379.
(48) The theoretical model assumes the components to be monodisperse, therefore the predictions for the UCST can be affected by the choice of the theoretical monodisperse M value, for example, whether it is taken to be the experimental M_w value or the M_n value. The results quoted here come by taking the average of these two choices, $M = (M_w + M_n)/2$, which gives an intermediate result (i.e., UCST = 309 K). In the Supporting Information we discuss this more fully and estimate lower and upper "bounds" for the UCST to be 296 and 327 K, respectively.
(49) Myers, D. B.; Smith, R. A.; Katz, J.; Scott, R. L. *J. Phys. Chem.* **1966**, *70*, 3341.